WHAT AVALANCHE OBSERVATIONS TELL US ABOUT THE PERFORMANCE OF NUMERICAL MODELS

Peter Gauer[1,*], Nellie Sofie Body[1], Anniken Helene Aalerud[1]

[1]*Norwegian Geotechnical Institute, Norway*

ABSTRACT: Avalanche velocity is an important parameter to characterize the avalanche dynamic behavior. Observations imply that the maximum velocity of major avalanches scales with the total drop height. Combining this information with observations of runout and volume of major avalanches can provide hints on the choice of the empirical parameters of numerical avalanche models. To this end, a simple track geometry is used to test the performance of present-days avalanche models. The model tracks varied in drop height and mean steepness. The model results are compared with expected values of the maximum velocity and runout based on avalanche observations.

Keywords: avalanche observations, avalanche models, performance test

1. INTRODUCTION

Runout observations provide limited only constraints for the validation of the empirical parameters used in common present-day numerical avalanche models. This is demonstrated in Fig.1, which shows five simulations with a simple mass block model governed by the equation of motion:

$$\frac{dU}{dt} = g \sin\phi - a_{ret} \,, \qquad (1)$$

where

$$a_{ret} = a_0 g \cos\phi + a_2 U^2 \text{ or } a_{ret} = a_3 \,. \qquad (2)$$

Here, U is the velocity, dU/dt the acceleration, g the gravitational acceleration, and ϕ is the slope angle of the track. The model parameters for the retarding acceleration are the Coulomb-friction parameter a_0 and the turbulent frictional parameter a_2. Both parameters can be related to the parameters commonly used in the Voellmy-fluid type friction law: $a_0 \equiv \mu$ and $a_2 \equiv g/(\xi h_f)$, with the flow depth h_f, or $a_2 \equiv D/M$ in the case of the PCM-model (Voellmy, 1955; Perla et al., 1980). The simple mass block model is ideal for illustration purposes as it is easy to follow, and yet, the model is an admissible first-order approximation. For comparison also the case with a constant retarding acceleration, a_3, is considered.

In this example, all the simulations are forced to reach the expected α_m-point according to the statistical α-β-model (Lied and Bakkehøi, 1980), but depending on the choice of the empirical parameters they show very different velocity distributions along the track. Assuming a flow depth

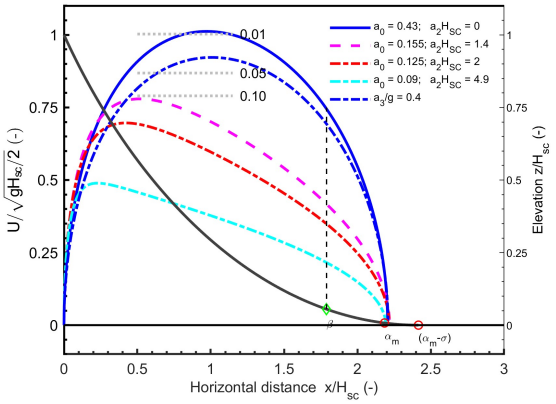


Figure 1: Velocity of a mass block moving with various parameter combinations of $\{a0; a_2 H_{SC}\}$ along a cycloidal track (black line; steepness in release area is $\phi_0 = 45°$) and reaching the α_m-point. Velocity and length are scaled with the total drop height H_{SC}. The gray dotted lines mark the probability of exceedance of the scaled velocity based on observations (c.f. Fig. 2 a)

h_f of 2 m and a drop height $H_{SC} = 1000$ m, the corresponding Voellmy parameters $\{\mu, \xi\}$ are $\{0.43, \infty\}$, $\left\{0.155, 3500\ \mathrm{m\,s^{-2}}\right\}$, $\left\{0.13, 2450\ \mathrm{m\,s^{-2}}\right\}$, and $\left\{0.09, 1000\ \mathrm{m\,s^{-2}}\right\}$. This choice of the parameters is inspired by values like $\mu = 0.155$ or $\xi \approx 1000\,\mathrm{m\,s^{-2}}$, or $a_2 H_{SC} = 2$, which can be found in the literature (e.g., Buser and Frutiger, 1980; Bakkehøi et al., 1983; Perla et al., 1980). However, those authors only focused on runout observations as constraint. For comparison, a simulation with a constant retarding acceleration is included too.

In all cases with a pronounced velocity dependency of the friction low, the parameter choice should depend on the drop height.

The differences in the predicted velocities can be crucial for the delimitation of endangered areas or the design of mitigation measures. The latter case is considered in the following example. Simple dimensioning criteria for avalanche catching dams re-

*Corresponding author address:
Peter Gauer, Norwegian Geotechnical Institute,
P.O. Box 3930 Ullevl Stadion, NO–0806 Oslo, Norway
Tel: ++47 45 27 47 43; Fax: ++47 22 23 04 48; E-mail: pg@ngi.no

late the required height of the free board H_{fb} to the avalanche velocity (see for example Chapter 8.4 in Rudolf-Miklau et al., 2014).

$$H_{fb} = \frac{U^2}{2g\lambda} + h_f \tag{3}$$

where λ is an empirical constant typically set to a value between 1 and 3, depending on the avalanche type (dry or wet). In the case of the example in Fig. 1, the avalanches, stopping at the α_m-point, still have a scaled velocity $U/\sqrt{gH_{SC}/2}$ of approximately 0.75, 0.70, 0.41, 0.35, or 0.22 at the β-point. If one were to plan a catching dam at the β-point, one could directly relate the required free board H_{fb} to the drop height H_{SC}

$$H_{fb} \approx f_v \frac{H_{SC}}{4\lambda} + h_f \tag{4}$$

where the factor f_v in our examples is 0.56, 0.49, 0.17, 0.12, or 0.05, respectively. That is, the design dam height may differ by a factor up to 10 or more, depending on the choice of the model parameters.

Furthermore, the predicted avalanche runtime, which is an important design parameter for some temporal mitigation measures such as automated road closures, may differ considerably with the choice of the friction parameters. In our example, the non-dimensional runtime, $t_{av}/\sqrt{H_{SC}/g}$, varies between approximately 6 and 13. This factor may determine wether an automated road closure is feasible or not. These are only two examples to show that not only the prediction of the runout is important but also the correct prediction of the velocity along whole track.

2. OBSERVATION

Therefore, velocity observations that could constrain model calibrations are desirable. Fig. 2 a shows the exceedance probabilities (i.e. the probability to observe a value larger than a given one) for a series of observed $U_{max}/\sqrt{gH_{SC}/2}$ (McClung and Gauer, 2018) and expected α values according to the α-β-model (Lied and Bakkehøi, 1980). The assumption of the empirical α-β-model is that the data behind it reflect rare avalanches, that is events with return periods of the order of 100 years. With this in mind, one might be tempted to multiply the exceedance probability in Figure 2 b by a factor of the order of 10^{-2} to obtain annual probabilities. However, this is a crude approximation. The complementary cumulative distribution function (CCDF) of U_{max} can be approximated reasonably well by a Generalized Extreme Value (GEV) distribution. Here and in the following, the term “major avalanche” is used in the sense that these avalanches have return periods of at least several years and can be considered large relative to the path, but not necessary the most extreme.

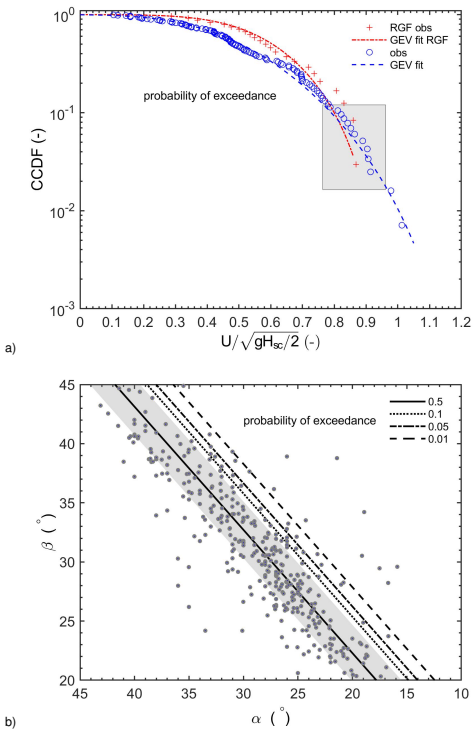


Figure 2: Complementary Cumulative Distribution Function (CCDF, survivor function) of observed values of $U_{max}/\sqrt{gH_{SC}/2}$ at Ryggfonn and for major avalanches at various locations. The gray rectangle indicates a region that covers typical rare events (cf. Fig. 3 b; and b) estimated exceedance probability of α versus β according to the α-β-model ($\alpha_m = 0.96\beta - 1.4°$; gray shaded area indicates $\alpha_m \pm \sigma$-range; for explanation see Lied and Bakkehøi, 1980).

Fig. 3 a shows the calculated (dimensionless) velocity of a mass block moving with a constant retarding acceleration along a cycloidal track. The retarding acceleration is chosen in such a way that the mass block stops at the β-point (which is close to the $\alpha_m + \sigma$-point), the α_m-point, or the $(\alpha_m - \sigma)$-point respectively. The light gray polygon indicates expected ranges for major avalanches according to the observations in Fig. 2. Fig. 3 b shows corresponding avalanche observations from major events with drop heights between 100 m and 1200 m. These observations have implication for the choice of model parameters as further discussed in the next section.

Fig. 4 shows a collection of observed deposition volumes. They show an increasing trend with drop height.

3. MODEL TESTS

3.1. Method

As mentioned, avalanche velocity is an important parameter to characterize the dynamic behavior. Observations imply that the velocity and especially the maximum velocity of major avalanches scale with the total drop height H_{SC}, that is $U_{max} \sim \sqrt{gH_{sc}/2}$ (McClung and Gauer, 2018; Gauer, 2018, 2014). Combined with estimates on the expected

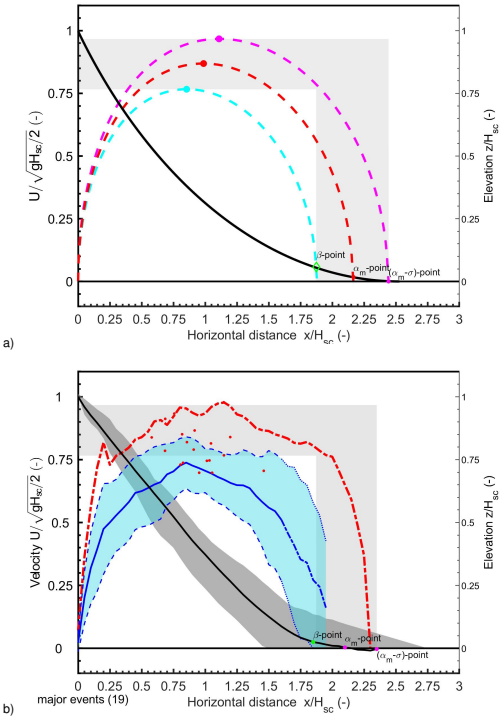


Figure 3: Scaling behavior of the front velocity of major avalanches combined with runout estimates. a) based on analytical calculations (cycloidal track and constant retarding accelerations; $\phi_0 = 48°$) and b) corresponding avalanche observations from major events. The blue line shows the mean, the shaded area the $\pm\sigma$-range and the red dashed line the observed maximum derived from observations along the track. The black line represents a "mean path" geometry and the dark gray shaded area the envelope of all path geometries. The light grey polygon provides a reference from Fig. 2.

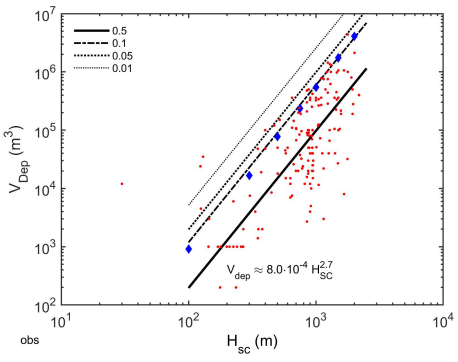


Figure 4: Observed avalanche deposits of "major events" versus total drop height H_{SC} (for references to the data see Gauer et al., 2010). ♦ indicate the volumes used in the model simulations in the next section. The lines show the estimated exceedance probabilities derived from the observations.

runout of major avalanches, e.g., by using statistical models, these observations provide implications for the choice of the empirical parameters used in numerical avalanche models. Like for the Voellmy-type friction models that find application in most of the present-day avalanche models.

Using a simple parabolic track, model performance can be tested. To this end, simulations were performed on slightly channelized parabolic tracks

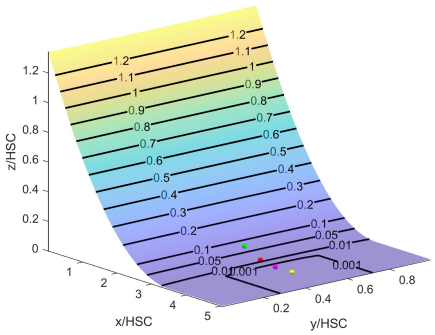


Figure 5: Model grid; the (•) mark the β-, α_m-, $(\alpha_m - \sigma)$-, and $(\alpha_m - 2\sigma)$-point.

where the thalweg is given by

$$z_1/H_{SC} = a(x/H_{SC})^2 + b(x/H_{SC}) + c \qquad (5)$$

and

$$z(x, y) = z_1(1 + f(y)) \,. \qquad (6)$$

Here, $f(y)$ defines the degree of canalization. Using a slight canalization should reduce lateral spreading, which is caused by numerical diffusion and therefore is an artifact. The parameter a, b, c are determined by the initial slope angle ϕ_0, which is also a proxy of the mean slope angle $\beta \approx 0.72\phi_0 - 1.4°$ (for explanations see Gauer, 2018). Fig. 5 shows an example grid.

At the low point, the track is horizontally extended. The initial volume is adjusted according to expected deposition volumes (see Fig. 4). The corresponding release areas are located above the actual track (i.e. $z_{SC} > 1$) with an assumed fracture depths $D_{frac} \approx [1\,\text{m}, 1.5\,\text{m}, 2\,\text{m}] \cdot \cos\phi_0$ and a constant slope angle ϕ_0 given by the initial tangent of the track.

The simulations were done with the commercial version of RAMMS:avalanche (version 1.7.20; (Christen et al., 2010)) and the MoT-Voellmy model (Version 2020-05-12, (Issler et al., 2023)).

The RAMMS friction parameters are chosen according to standard values (Bartelt et al., 2017) corresponding to the respective volume class. However, only the highest elevation class is used, which gives the lowest friction values—that is, they should favor longer runouts and higher velocities. The parameter for the MoT-Voellmy model are chosen similarly.

In addition, simulations were done with the SAMOS-solver for dense flow (Sampl and Granig, 2009) including entrainment, however, with a modified friction law that favors Coulomb-type behavior:

$$\tau_b = \mu\,\rho_f\,g\,h_f\cos\phi + C_D\rho_a\,U^2 + \tau_c \max\left(\exp\left(-u^2/25\right), \exp\left(-10h_f^2\right)\right) , \qquad (7)$$

where h_f is the flow depth, the avalanche density $\rho_f = [100, 200]\,\mathrm{kg\,m^{-3}}$, the Coulomb friction factor $\mu = 0.3$, $C_D\rho_a = 0.05\,\mathrm{kg\,m^{-3}}$ and $\tau_c = 100\,\mathrm{Pa}$. The second term on the right accounts for some air drag and the last term on the right introduces some cohesion, which should mainly suppress spreading of very shallow flows. This friction law is inspired by the simple model tests in Gauer (2020). The entrainment is set to $\leq 300\,\mathrm{kg\,m^{-2}}$.

3.2. Results

Using the simple parabolic track, model performance can be tested as shown in Fig. 6 and Fig. 8. Here, we focus mainly on the RAMMS (Christen et al., 2010) as it is probably one of the (if not the) most used model by practitioners at present. Fig. 6 shows an example of the kind of simulations and show the overall maximum values of the simulation at a given grid point.

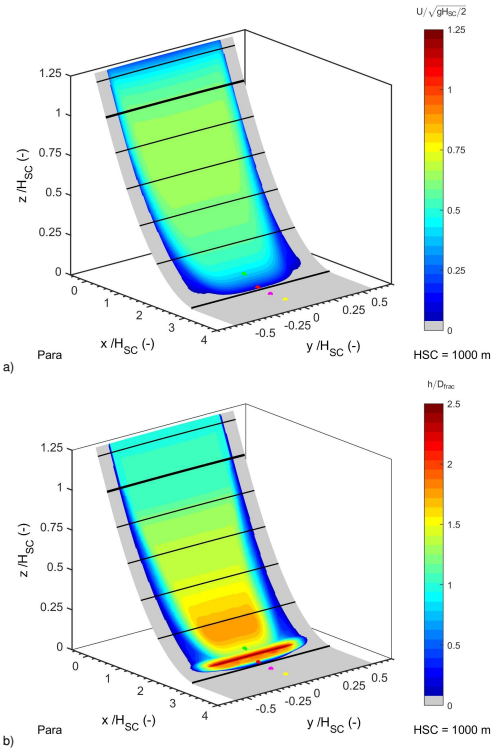


Figure 6: Simulation with RAMMS on a parabolic track: a) maximum velocity and b) maximum flow depth. The velocity is scaled as $U_{SC} = U_{max}/\sqrt{gH_{sc}/2}$ and the flow depth as $h = h_f/\mathrm{D}_{frac}$, where D_{frac} is the initial fracture depth.

Fig. 7 shows a comparison of avalanche simulations with RAMMS for different drop heights $H_{SC} = [100, 300, 500, 750, 1000, 1500, 2000]$ m. The volumes were adjusted according to expected deposition volumes (see Fig. 4). The corresponding release areas are located above the actual track with an assumed a fracture depth $\mathrm{D}_{frac} = 2\cos\phi_0$ m and a constant slope angle (in this case $\phi_0 = 35°$) given by the initial tangent of the track; the mean slope

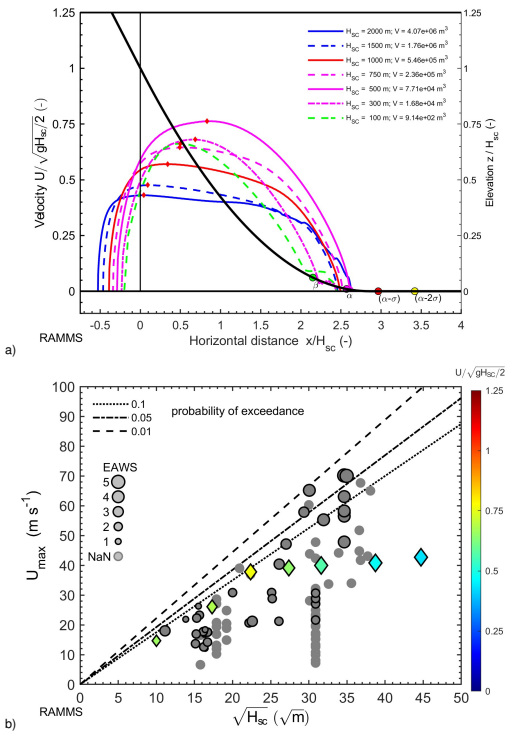


Figure 7: a) Simulated velocities with RAMMS along the thalweg for seven different drop heights. The maxima are marked with (⧫). The release volumes are adjusted to the drop height, the fracture depth is set to 1.64 m and $\phi_0 = 35°$. As a reference, the β-, α_m-, $(\alpha - 1\sigma)$- and $(\alpha_m - 2\sigma)$-point are shown (for explanation see Lied and Bakkehøi, 1980). b) Simulated maximum velocity, U_{max}, versus square root of the drop height, $\sqrt{H_{sc}}$, marked by (⧫); the color illustrates the scaled velocity $U_{SC} = U_{max}/\sqrt{gH_{sc}/2}$ and the marker size corresponds to the EAWS avalanche size classes. The lines show the estimated exceedance probabilities derived from observations shown in gray.

angle is $\beta \approx 23.6°$.

As can be seen in Fig. 7 a the runout ends approximately at the mean expected α_m-angle according to the α-β-model, even though the large volumes used could suggest that these simulations represent more extreme events. For drop heights up-to around 750 m, the simulated maximum velocities are in the range of rare events (cf. panel b). For drop heights above, the maximum velocity reaches a terminal velocity, which is not reflected in the observations. For drop heights larger than 1000 m, the simulations underestimate the velocities significantly compared to the observations of major events. This is a typical problem for models based on the Voellmy-fluid rheology (see also discussions in Gauer, 2014, 2013, 2018). However, also for drop heights smaller than 1000 m a subtle difference seems to exist as the simulated maximum velocity tends to be obtained earlier in the path than suggested by observations.

Fig. 8 shows the corresponding simulation as shown in Fig. 6 for the MoT-Voellmy model. The results are comparable to those from RAMMS, however, in this case the simulation suggests also some spurious numerical artifacts.

As mentioned above, the combination of runout

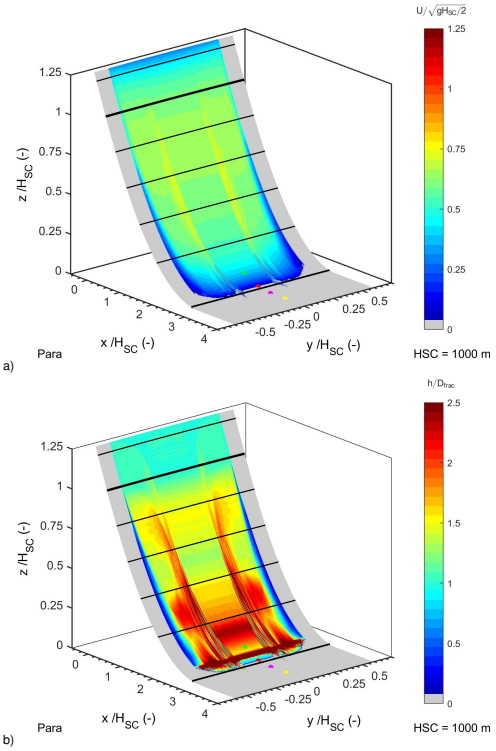


Figure 8: Simulation with MoT-Voellmy on a parabolic tracks: a) maximum velocity and b) maximum flow depth. The velocity is scaled by $U_{SC} = U_{max}/\sqrt{gH_{sc}/2}$ and the flow depth by $h = h_f/D_{frac}$, where D_{frac} is the initial fracture depth (simulation to t = 100 s; build version MoT-Voellmy.2020-05-12.exe).

observations and velocity scaling can provide a more stringent constraint to the choice of the empirical model parameters for the commonly used friction laws. Choosing a simple track geometry and the use of expected runout and maximum velocities along the track can therefore give a fast impression of model performance versus observations depending on the model parameters.

The approach is exemplified in (Gauer, 2018, 2020). Fig. 9, Fig. 10, and Fig. 11, show results obtained with a simple mass block model that accounts for mass entrainment (Gauer, 2020). Although only a first order approximation, the model captures the observations for “major” dry-mixed avalanches reasonably well. Therefore, the figures give a reference for the 2D-simulations shown below in this section. As the model is basically scale invariant regarding the drop height H_{SC}, Fig. 11 should be similar for various drop heights. The colors and isolines indicate the velocity distribution along the horizontal distance for simulations along tracks with varying steepness, ϕ_0 (or $\beta \approx 0.72\phi_0 - 1.4°$). For the illustration, the data are interpolated.

Fig. 13 gives now a summary of the simulated runout angles for the 2D models. As indicated, the models seem to capture the expected runout according to the observations. However, one could have expected longer runouts considering the simulation setup that should have favoured higher velocities and longer runout for the Voellmy-type models. Also, it can be noticed that there is a slight in-

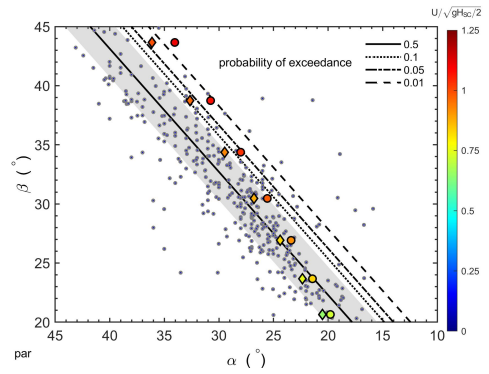


Figure 9: Simulated runout marked by the α-angle and maximum velocity (color coded) on a parabolic track with the mean slope angle, β, as parameter. (•) marks runs with entrainment height He = 0.25 m and (⧫) those with He = 0.5 m. Observations are shown as gray dots. Estimated exceedance probabilities of α versus β, according to the α-β-model $\alpha_m = 0.96\beta - 1.4°$ (Lied and Bakkehøi, 1980); gray shaded area $\alpha_m \pm \sigma$.

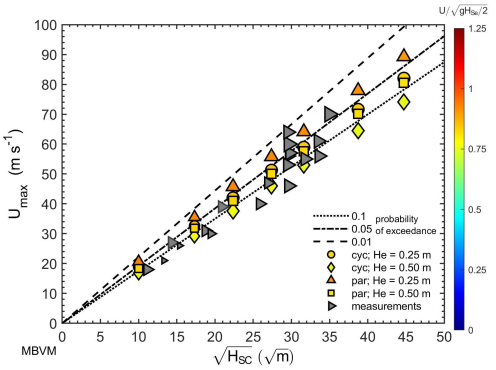


Figure 10: Simulated maximum velocity, U_{max}, versus square root of the drop height, $\sqrt{H_{SC}}$. The color illustrates the scaled velocity, $U_{SC} = U_{max}/\sqrt{gH_{SC}/2}$. The figure shows example calculations for a cycloidal and parabolic track and two erosion depths. The initial slope angle ϕ_0 of the tracks is 40°. The gray triangles depict measured maximum front-velocities from ”major avalanche events” in various tracks (see Fig. 3). The lines depict the probability of exceedance.

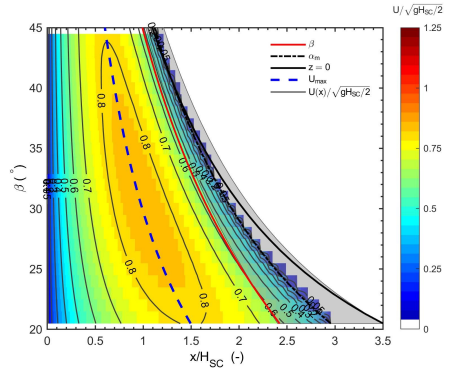


Figure 11: MBVM (Mass Block with Variable Mass): Normalized velocity, $U/\sqrt{gH_{SC}/2}$; iso-lines of scaled avalanche velocities on some parabolic tracks with different steepness given by the β-angle. Runout length given to hit the average runout angle α_m corresponding to the α-β-model (Lied and Bakkehøi, 1980). Also marked are corresponding positions of β, α_m, and where z becomes zero. Gray shaded area shows $\alpha_m \pm \sigma$ range.

crease in runout length with increasing slope steepness. This is especially obvious in the Coulomb friction dominated SAMOS$_{CCDTM2}$ model. Here, the increase is pronounced for lower drop heights, which can be observed in Fig. 14.

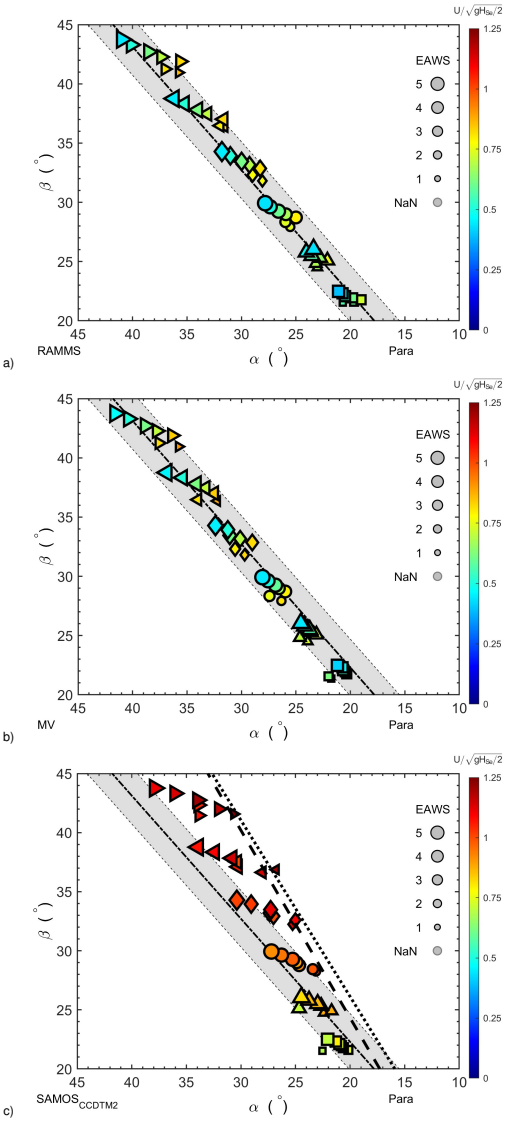


Figure 12: Simulated runout marked by the α-angle and maximum velocity (color coded) on a parabolic track with the mean slope angle, β (varying symbol) as parameter and vertical release depth HS = 1.5 m. Expected runout angle α versus β, according to the α-β-model $\alpha_m = 0.96\beta - 1.4°$ (Lied and Bakkehøi, 1980); gray shaded area $\pm\sigma$. Symbol size gives an impression of the avalanche size according to EAWS volume classification. a) RAMMS; b) MoT-Voellmy; c) SAMOS$_{CCDTM2}$. The additional dotted and dashed lines in c) show the α-β-model for Colorado and the Sierra Nevada, respectively (c.f. McClung and Mears, 1991).

Fig. 14 shows plots corresponding to Fig. 11. The values in all cases are taken along the center line of the track and then interpolated. On a first glance, the results suggest that the models are capable to capture the runout distances reasonably well, although one could have expected even longer runouts with respect to the model setting, see also Fig. 12.

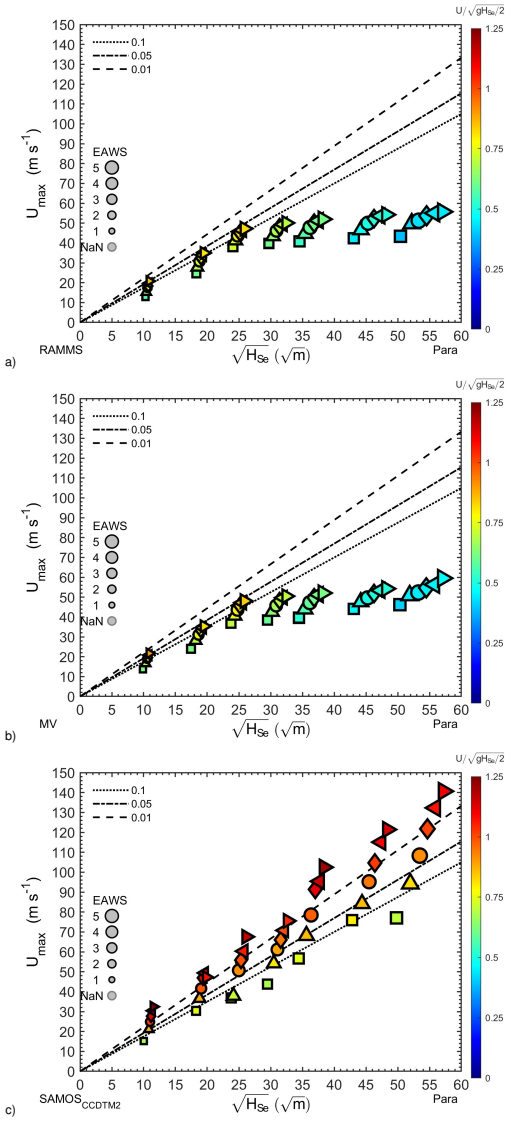


Figure 13: Simulated maximum velocity, U_{max}, versus square root of the effective drop height $\sqrt{H_{Se}}$ (i.e., including the height of the release area) with the mean slope angle, β as parameter (varying symbols; for comparison see Fig. 12) and vertical release depth HS = 1.5 m. The color illustrates the scaled velocity $U_{SC} = U_{max}/\sqrt{gH_{SC}/2}$. a) RAMMS; b) MoT-Voellmy; c) SAMOS$_{CCDTM2}$.

There are, however, noticeable difference between the predicted maximum velocities and those observed, especially for avalanche drops heights larger 1000 m. This is also very well reflected in Fig. 13. But also for smaller drop heights it seems there are differences in the velocity profiles. That is, the simulations reach its maximum velocity early on and underestimate the velocity the lower part of the track as mentioned before. RAMMS and MoT-Voellmy show quite similar behaviour. Both model show a pronounced drop height dependency, which is not reflected in observations of major avalanches. The drop height dependency is less in the more Coulomb-type model implemented in the SAMOS-solver.

4. CONCLUDING REMARKS

In this paper, a simple track geometry was used to test the performance of present days avalanche models. The model tracks varied in drop height and mean steepness. The model results were compared with expected values of the maximum velocity and runout based on avalanche observations.

On a first glance, the results suggest that the models are capable to capture the runout distances reasonably well, although one could have expected even longer runouts with respect to the model setting. There are, however, noticeable difference between the predicted maximum velocities and those observed, especially for avalanche drops heights larger 1000 m. Also for smaller drop heights, it seems there are differences in the velocity profiles and that the simulation reaches its maximum velocity early on and underestimate the velocity the lower part of the track.

Here, we focused mainly on RAMMS and on MOT-Voellmy, but similar results are expected and are known for other models using the Voellmy-rheology too, like DAN3D (Aaron et al., 2016; Conlan et al., 2018) or SAMOS-AT (Sampl and Granig, 2009).

The more Coulomb-type variant of SAMOS presented here shows less velocity dependency of the friction term and is better capable to reproduce the higher observed velocities for larger drop heights. There is, however, tendency to show longer runouts than expected by the α-β-model for Norway for steeper paths, at least for the parameters used here. On the other hand, these runouts are still in accordance with observation from Colorado or Sierra Nevada.

At this point, model developers could argue that the Voellmy-rheology focuses mainly on the prediction the dense- (or may be the slightly fluidized-) part of the avalanche, and that the observations are uncertain and include also events of highly fluidized- or powder snow events. This refutation might be justified, but the observations include avalanches that are highly relevant for practitioners concerned with hazard mapping and mitigation. Then practitioners need to ask themselves, Are we using the right tools? Are models that better account for varying flow-regimes and mass exchange needed?

ACKNOWLEDGMENTS

Parts of this research was financially supported by the Norwegian Ministry of Oil and Energy through the project grant “R&D Snow avalanches 2017–2019 & 2020–2023” to NGI, administrated by the Norwegian Water Resources and Energy Directorate (NVE).

REFERENCES

Aaron, J., Conlan, M., Johnston, K., Gauthier, D., and McDougall, D. (2016). Adapting and calibrating the dan3d dynamic model for north american snow avalanche runout modelling. In *International Snow Science Workshop 2016 Proceedings, Breckenridge, CO, USA*.

Bakkehøi, S., Domaas, U., and Lied, K. (1983). Calculation of snow avalanche runout distance. *Annals of Glaciology*, 4:24–29.

Bartelt, P., Bühler, Y., Christen, M., Deubelbeiss, Y., Salz, M., Schneider, M., and Schumacher, L. (2017). *RAMMS User Manual v.1.7.0 Avalanche*. WSL Institute for Snow and Avalanche Research SLF.

Buser, O. and Frutiger, H. (1980). Observed maximum run-out distance of snow avalanches and the determination of the friction coefficients μ and ξ. *Journal of Glaciology*, 26(94):121–130.

Christen, M., Kowalski, J., and Bartelt, P. (2010). RAMMS: Numerical simulation of dense snow avalanches in three-dimensional terrain. *Cold Regions Science and Technology*, 63:1–14.

Conlan, M., Aaron, J., Johnston, K., Gauthier, D., and McDougall, S. (2018). Dan3D model parameters for snow avalanche case studies in Western Canada. In *Dan3D Model Parameters for Snow Avalanche Case Studies in Western Canada*, pages 783–787.

Gauer, P. (2013). Comparison of avalanche front velocity measurements: supplementary energy considerations. *Cold Regions Science and Technology*, 96:17–22.

Gauer, P. (2014). Comparison of avalanche front velocity measurements and implications for avalanche models. *Cold Regions Science and Technology*, 97:132–150.

Gauer, P. (2018). Considerations on scaling behavior in avalanche flow along cycloidal and parabolic tracks. *Cold Regions Science and Technology*, 151:34–46.

Gauer, P. (2020). Considerations on scaling behavior in avalanche flow: Implementation in a simple mass block model. *Cold Regions Science and Technology*, 180:103165.

Gauer, P., Kronholm, K., Lied, K., Kristensen, K., and Bakkehøi, S. (2010). Can we learn more from the data underlying the statistical α-β model with respect to the dynamical behavior of avalanches? *Cold Regions Science and Technology*, 62:42–54.

Issler, D., Gledisch Giss, K., Gauer, P., Glimsdal, S., Domaas, U., and Sverdrup-Thygeson, K. (submitted 2023). NAKSIN – a New Approach to Snow Avalanche Hazard Indication Mapping in Norway. *Cold Regions Science and Technology*.

Lied, K. and Bakkehøi, S. (1980). Empirical calculations of snow-avalanche run-out distance based on topographic parameters. *Journal of Glaciology*, 26(94):165–177.

McClung, D. M. and Gauer, P. (2018). Maximum frontal speeds, alpha angles and deposit volumes of flowing snow avalanches. *Cold Regions Science and Technology*, 153:78–85.

McClung, D. M. and Mears, A. I. (1991). Extreme value prediction of snow avalanche runout. *Cold Regions Science and Technology*, 19(2):163–175.

Perla, R., Cheng, T. T., and McClung, D. M. (1980). A two-parameter model of snow-avalanche motion. *Journal of Glaciology*, 26(94):119–207.

Rudolf-Miklau, F., Sauermoser, S., and Mears, A. I., editors (2014). *The Technical Avalanche Protection Handbook*. Ernst & Sohn.

Sampl, P. and Granig, M. (2009). Avalanche simulation with SAMOS-AT. In *Proceedings of the International Snow Science Workshop, Davos*, pages 519–523.

Voellmy, A. (1955). Über die Zerstörungskraft von Lawinen. *Schweizerische Bauzeitung*, Sonderdruck aus dem 73. Jahrgang(12, 15, 17, 19 und 37):1–25.

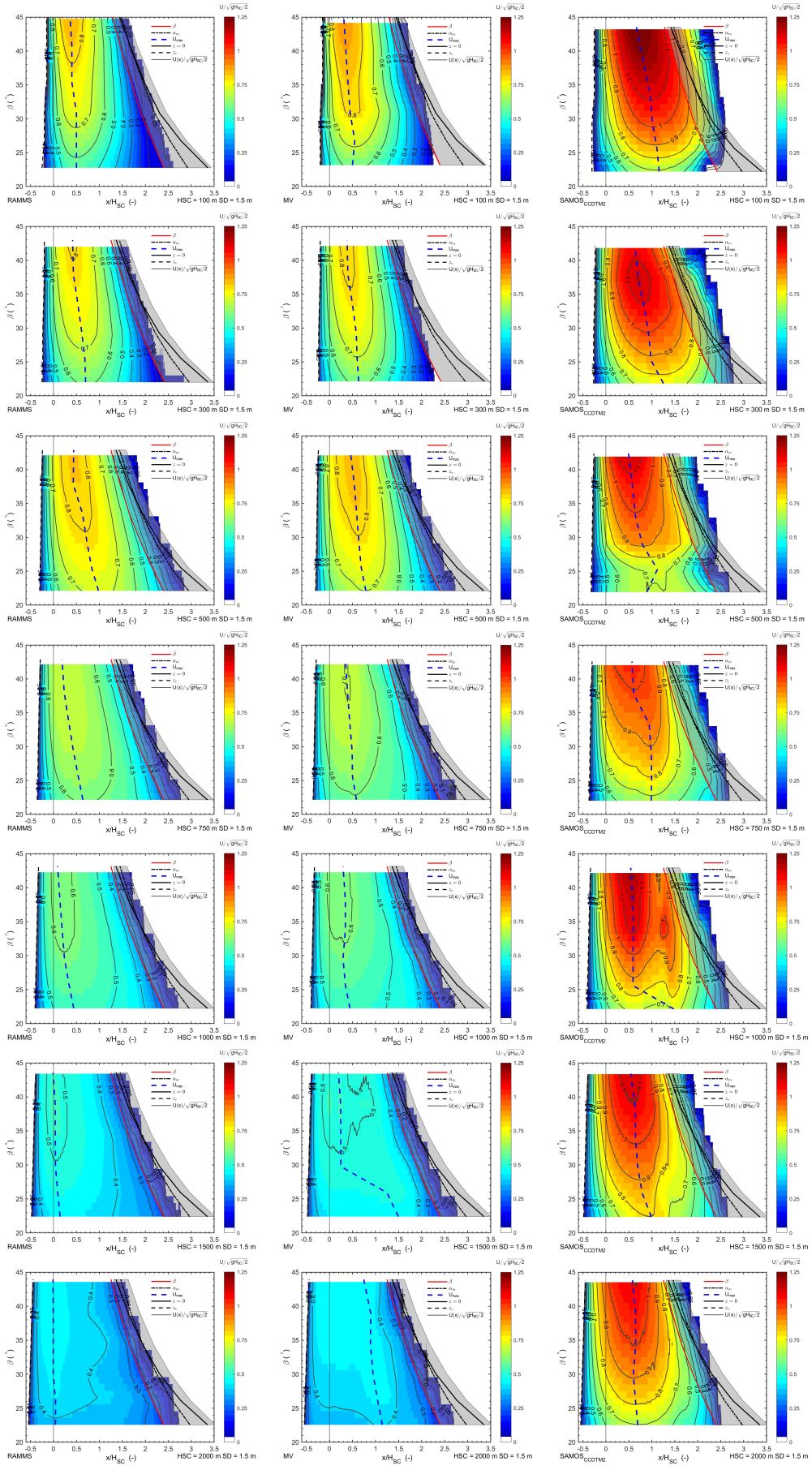


Figure 14: Maximum normalized velocity, $U/\sqrt{gH_{SC}/2}$, along the center line for various drop heights, H_{SC} = [100, 500, 750, 1000, 1500, 2000] m (top to bottom) for the models RAMMS, MoT-Voellmy, and SAMOS$_{CCDTM2}$